LIMNOLOGY
and
OCEANOGRAPHY: METHODS

ASLO

Limnol. Oceanogr.: Methods 2025

doi: 10.1002/lom3.10684

NEW METHODS

DISCO: A low-cost device-instrumented Secchi disk for water clarity observations

Gaia Donini, Sebastiano Piccolroaz*

Department of Civil, Environmental and Mechanical Engineering, University of Trento, Trento, Italy

Abstract

Water clarity regulates irradiance penetration in aquatic environments, influencing physical and biological dynamics: irradiance penetration affects heat transfer in the water column and provides energy through photosynthetically active radiation (PAR) in the euphotic zone, which is vital for light-dependent organisms. The ability to accurately assess water clarity is therefore important in several aquatic science contexts, from data analysis and process interpretation to modeling. Common metrics used to quantify water clarity include the vertical irradiance attenuation coefficient K, a measure of irradiance penetration, and the Secchi disk depth (z_{SD}), a measure of water visibility. The enduring simplicity and low cost of the Secchi disk has made it a global standard for measuring water clarity for almost two centuries. In contrast, K is typically determined using expensive instruments that measure underwater irradiance profiles. This highlights the need for innovative, cost-effective methods that integrate both types of measurements. Here we present DISCO, a low-cost, easy-to-build instrument that retains the traditional appearance of a Secchi disk, and is equipped with photoresistors (also known as light-dependent resistors, LDRs) both looking upwards and downwards for planar irradiance measurements. DISCO is also equipped with low-cost temperature and pressure sensors, all connected to an ArduinoUNO board. DISCO was tested in two mountain lakes together with high resolution PAR, temperature and pressure sensors to calibrate the LDRs and validate its performance. The results show that the proposed instrument is able to measure the irradiance attenuation coefficients with an error of less than 10% compared to the reference PAR sensor.

Natural waters are populated by suspended matter, including phytoplankton, zooplankton, sediments, and, more recently, microplastics (Nava et al. 2023). Together with colored dissolved organic matter (CDOM), all these suspended particles collectively regulate water transparency and color (Cristofor et al. 1994; Yang et al. 2022; Meyer et al. 2024). The radiative transfer equation describes the attenuation of radiance as it penetrates the water column. Assuming a homogeneous medium where absorption dominates over scattering, and focusing on the planar downwelling and upwelling integrated radiance (i.e., irradiance), the equation simplifies to the Beer–Bouguer–Lambert law (Beer 1852), a condition commonly observed in the field

$$I = I_0 e^{-Kz} \tag{1}$$

where I_0 is the irradiance just below the surface, z [m] is the water depth (positive downward), K [1/m] is the average vertical attenuation coefficient representing the rate at which irradiance decreases as it penetrates into a body of water, and I is the irradiance at depth z after passing through the water column. The unit of measurement for I varies depending on the specific field of application and the context of investigation: I can denote an energy flux density [W/m^2], an illuminant density [lx] (i.e., lumen per square meter), or a photon flux density [μmol/m^2 s] (Kuroiwa et al. 1983), where the term density is used here to indicate normalization per unit area. The latter is typically used when referring to Photosynthetically Active

*Correspondence: s.piccolroaz@unitn.it

Data Availability Statement: The data that support the findings of this study are openly available in Zenodo at https://zenodo.org/records/14419602.
Associate editor: Gordon T. Taylor

Radiation (PAR), that is, the portion of the electromagnetic spectrum required for photosynthesis, which lies between 400 and 700 nm in wavelength, thus falling within the visible light spectrum.

The attenuation coefficient K is the result of the absorption, reflection and scattering due to the suspended and dissolved matter in water and the water itself (Kirk 2010). The attenuation coefficient is therefore a measure of water clarity, a key water quality parameter that influences various physical and biological processes. For example, water clarity influences the radiative heating of the water column by modulating its absorption with depth. As shortwave radiation penetrates the water and interacts with suspended and dissolved matter, it creates layers of differing temperatures, hence determining the thermal structure and stratification of the water column (Houser 2006; Rose et al. 2016; Pilla et al. 2018; Bouffard and Wüest 2019; Liu et al. 2022). In turn, thermal stratification affects the vertical distribution of heat, momentum and dissolved substances, with implications for the overall balance of the aquatic ecosystem (Pöschke et al. 2015; Lin et al. 2021; Dresti et al. 2023). Water clarity also plays a direct role in shaping the ecosystem and biological processes. Photoautotrophic organisms, for example, such as phytoplankton, cyanobacteria, and aquatic plants rely on light, or more specifically PAR, to acquire energy for growth and reproduction through photosynthesis. These organisms live in the euphotic zone, a layer bounded by the water surface and the euphotic depth, the latter being defined as the depth at which PAR is reduced to 1% of the its value at the surface (Kirk 2010). The euphotic depth can be readily determined using Eq. 1 as $z_e = -\frac{\ln(0.01)}{K} = \frac{4.605}{K}$, highlighting its dependence on the attenuation coefficient K, and thus on the clarity of the water. It should be noted that, in shallow lakes, where the euphotic zone extends down to the lake bottom, another important source of light for photosynthesis is the upwelling irradiance scattered by the bottom (Kirk 1977), which also influences the attenuation coefficient K of the water column. Notably, the presence of photoautotrophic organisms within the euphotic zone can trigger a feedback mechanism, reducing water clarity and consequently limiting the depth of the euphotic zone due to their presence (Persson and Jones 2008; Rinke et al. 2010).

The feedback effects of bio-ecological processes on water clarity pose a challenge for lake models to accurately capture the thermo-hydrodynamics of the water body (Hocking and Straškraba 1999; Rinke et al. 2010; Subin et al. 2012; López Moreira et al. 2021; Pilla and Couture 2021). Not surprisingly, independent lake modeling analyses confirmed the key importance of the attenuation coefficient, and more generally the parameterization of absorption in the water column, as a strong control on the lake mixing regime, lake ecosystem functioning, and lake-climate interaction (Persson and Jones 2008; Heiskanen et al. 2015). This highlights the need to couple thermo-hydrodynamic (i.e., physically based) lake models with biogeochemical lake models and hydrological catchment models, in order to explicitly modeling water clarity based on internal lake dynamics and external nutrients loads (Piccolroaz et al. 2024). Although this multi-level coupling should be common practice, especially in the context of climate change prediction analysis (Persson and Jones 2008; Subin et al. 2012), it is not trivial to implement and is therefore often overlooked. In fact, water clarity is often modeled in an oversimplified way in lake models, but this could not be otherwise given the general (scarce) availability of data and the complexity of accounting for the different processes and feedback between them. Not infrequently, irradiance penetration in the water column is simulated by considering a constant value for the attenuation coefficient K (*see* e.g., Tyler 1968; Persson and Jones 2008; Subin et al. 2012; Markelov et al. 2019) without considering its variation over the year due to variable suspended matter types and concentrations, and/or assuming a monochromatic light source, thus neglecting the dependence of irradiance on wavelength across the light spectrum (Piccolroaz et al. 2024).

The irradiance attenuation coefficient K can be evaluated directly by measuring vertical irradiance profiles. If a radiometer is equipped with a cosine collector, the downward or upward planar irradiance is measured (when the sensor is oriented upward or downward, respectively), the cosine collector being a detector that allows the angular distribution of incoming radiation orthogonal to the radiometer surface to be correctly accounted for. Alternatively, spherical collectors are used to measure scalar irradiance (i.e., irradiance from all directions). When a hyperspectral radiometer is available, wavelength-dependent attenuation coefficients can be assessed (Bouffard et al. 2019), otherwise if single bands sensors are available the corresponding attenuation coefficient is evaluated under the hypothesis of a monochromatic light. Normally, PAR sensors are employed, which allow to estimate K for the integrated light spectrum in the wavebands relevant for photosynthesis (Weiskerger et al. 2018). When it is possible to determine K from an irradiance profile, this is the preferred option since it is the relevant measure of water clarity for most research in aquatic ecosystems (Turner et al. 2023). However, this may be hampered by the relatively high cost of some radiometers, and other options may be considered. Measurements such as chlorophyll-a concentration, total suspended solids concentration, turbidity and Secchi disk depth z_{SD} can be used as alternative metrics of water clarity (Turner et al. 2023), which are relatively easier and cheaper to collect, but do not provide the same integrated and complete information as K. In some cases, K can be empirically estimated as a function of other water quality metrics, the most common of which is certainly z_{SD}. The relationship between K and z_{SD} depends on the substances in water, due to their different ability to scatter light (Turner et al. 2023). The Secchi disk depth is a measurement of underwater visibility, which is obtained by lowering a standard disk into the water until it is

no longer visible and measuring the depth at which it disappears from sight (Secchi 1864). In limnological applications, a 20 cm diameter disk painted in black and white quarters is commonly used, while in marine applications a 30 cm diameter white disk is preferred (Aas et al. 2014). The Secchi disk was introduced in the mid-19th century by the Italian priest Pietro Angelo Secchi, from whom it takes its name, and has since become a standard water quality measurement (Wernand 2010) due to its simplicity and affordability, despite obvious subjective (e.g., experience and vision of the operator) and objective (e.g., intensity of the ambient light and waves on the free surface) factors that can affect the measurement (*see* Smith (2001) for a protocol for standardizing z_{SD} measurements). A recent overview of Secchi's legacy to aquatic optics has been provided by (Pitarch 2020), which also includes interesting historical notes and relevant information on factors influencing Secchi disk readings.

Nowadays, water clarity and other optical properties can also be measured using satellite remote sensing reflectance measurements, which are used to estimate the Secchi disk depth (Giardino et al. 2001; Lee et al. 2015; Pitarch et al. 2021). The most obvious advantages are related to the higher spatial and temporal coverage compared to in-situ measurements, which are still predominantly conducted manually and suffer from a significant labor burden, the under-representation of remote and difficult to access sites, and the so-called "fair weather bias," where sampling is not carried out in bad weather conditions (Rand et al. 2022). However, large and globally representative in-situ datasets are a fundamental requirement for the development and validation of bio-optical algorithms to support large-scale monitoring using satellite Earth observation technologies (Lehmann et al. 2023). In this respect, a desired goal is to be able to conduct sparse in-situ water clarity measurements, which are affordable, reliable, and effective in providing the necessary ground reference for satellite data calibration and validation. Advancements in technology have led to the development of a few do it yourself (DIY) instruments for water clarity measurements. An example is KdUINO (Bardaji et al. 2016), or its improved version KduPro (Rodero et al. 2022), a low-cost device consisting of a vertical array of photodiodes installed at discrete depths, which can be used to invert the Beer–Bouguer–Lambert law to obtain K. A Sensing Secchi Disk (SSD) (Brewin et al. 2024) has been recently developed in response to interest in measuring the attenuation coefficient without sacrificing Secchi depth measurement. The SSD is an Arduino-based instrument with spectral light, temperature, pressure, and GPS sensors encapsulated in epoxy resin and integrated into a mini-Secchi disk (Brewin et al. 2019). Parallel to this, the decreasing cost of sensors enabled the exploration of alternative approaches. For example, when the penetrating shortwave solar radiation is the dominant cause of vertical temperature change, paired water temperature sensors has been used to estimate K (Read et al. 2015). The simplicity and affordability of these devices make them suitable for citizen science initiatives, as demonstrated by the Secchi Disk Foundation (http://www.secchidiskfoundation.org/), which engages people around the world in hands-on marine science to educate while increasing our knowledge of the sea through the use of Secchi Disks for measuring water transparency.

Inspired by these experiences, in this study we propose DISCO, a low-cost Device-Instrumented Secchi disk for water Clarity Observations. DISCO is an easy-to-build DIY instrument that combines the classical Secchi disk measurement with the direct measurement of planar irradiance profiles. The underlying philosophy is to retain the standard Secchi disk measurement, providing continuity to existing databases often dating back several decades, while adding an objective estimate of the attenuation coefficient for PAR, hereinafter simply referred to as K. DISCO has the appearance of a classic 20 cm diameter black and white Secchi disk for limnological applications, with a housing underneath that contains the electronics, including: four upward-looking and four downward-looking photoresistors for irradiance measurement, a pressure sensor for vertical positioning of the instrument in the water column, and a temperature sensor that is always useful. The electronics are controlled by an ArduinoUNO board, and are designed to make it easy to replace sensors in the event of malfunction or damage. This makes DISCO particularly flexible for possible upgrades with new components and sensors, such as the use of a Bluetooth or WiFi connection to download data, a magnetic key to switch the device on/off, and the use of more complex spectral irradiance sensors as proposed in Brewin et al. (2024). The cost of DISCO is affordable (about 80 € for the electronics and 100 € for the case) and it is easy to build, even by non-electronics experts like the authors, allowing for potential widespread dissemination and application. To summarize, compared to the other DIY products described above, DISCO combines ease of construction and affordability with flexibility for sensor replacement and potential upgrades, supporting multiple sensors for uncertainty assessment, while retaining the characteristics of a standard Secchi disk.

Materials and procedures

Instrument overview

DISCO is a standard Secchi disk for freshwater applications, that is, a black and white plate of 20 cm diameter, integrated with electronic components for measuring downwelling and upwelling planar irradiance, pressure and temperature. In this way, the instrument combines the measurement of the standard Secchi disk depth with the measurement of irradiance profiles within the PAR range, from which it is possible to obtain the objective estimation of the irradiance attenuation coefficient for PAR K using Eq. 1. Simultaneously, water temperature profiles are recorded, as one of the most relevant monitoring variables.

With a total cost of about 180, including 80 for electronics and 100 for the housing, DISCO is an affordable device that

further benefits from simplicity in assembling the electronics and the housing. Details of DISCO's waterproof housing and of the electronics inside are given in the following sections, while the detailed list of materials used in the construction of DISCO and their prices can be found in Table 1.

Waterproof housing

The housing must be waterproof up to 2–3 bar (i.e., approximately 20–30 m water depth) to prevent water ingress, which could damage the electronics. It consists of two parts (*see* Fig. 1a–e): the lid, which has the appearance of the Secchi disk (Fig. 1b), and a compartment underneath to house the electronics (Fig. 1d). Both are made of PVC.

The lid is 20 cm in diameter, 2 cm thick, and painted in black and white quarters (Fig. 1b). In each one of the black or white quadrants, there is a 5 mm hole housing the four upward-looking photoresistors, also known as light-dependent resistors (LDRs). The holes are covered with a small square of glass about 2 cm × 2 cm, 2 mm thick, glued to the PVC. Glass was chosen over other options, such as Plexiglas, because it is more scratch-resistant and therefore retains its optical clarity over time, ensuring consistent light transmission for accurate measurements. Sealing paste is used inside the holes to hold the LDRs in place and block any internal light source (e.g., from the ArduinoUNO LEDs). An eyebolt, which is used to attach the rope for lowering the instrument into the water, is screwed into the center of the lid.

The lower compartment is a cylinder, 12.5 cm in external diameter and 8.5 cm high, closed at the bottom with a 1.5 cm thick disk and equipped with a 20 cm diameter and 2.5 cm thick annular flange at the top, to be connected to the lid to close the housing (Fig. 1a,d,e). In order to ensure waterproofing, the annular flange has two grooves, each 3 mm wide and 2.6 mm deep, along a circle of diameter 13.5 and 18.5 cm to accommodate two O-rings, each 3 mm in diameter. Seven screws, positioned between the O-rings, secure the lid to the flange. Similar to the lid, four holes covered by a small glass square at the bottom of the lower compartment house four downward-looking LDRs. There are two additional holes in the bottom of the lower compartment: one in the center where the pressure sensor is screwed in, and another on one side where a cable gland for the temperature sensor is located (Fig. 1c). Finally, there are four long screws at the bottom to prevent damage to the sensors and scratches on the glass protectors if the DISCO hits the bottom of the lake or when it is handled out of the water. These screws are also used to adjust the buoyancy of the housing, using ballast nuts.

A lathe was used to cut the lid, the annular flange, and the bottom disk from PVC panels. The same machine was also used to create the grooves. A male thread tap was employed to create the holes for the seven screws that secure the lid to the annular flange, the eyebolt, the pressure and temperature sensors, and the four screws at the bottom. The holes for the LDRs were made using a drill bit. Tangit glue was used for the PVC pieces, and Attak glue was used for the glass squares. The waterproofing of the housing costs approximately 100, though expenses could be reduced by using thinner PVC panels.

Table 1. List of materials used to build DISCO, including the number of pieces, nominal cost per piece, and total cost (in Euros).

Material	No. of Pieces	Unit cost [€]	Total cost [€]
ArduinoUNO Rev3 SMD	1	27.65	27.65
Adafruit Data Logging Shield	1	13.95	13.95
CdS NSL-19 M51 photoresistor	8	0.95	7.60
Multiplexer 74HC4051	1	2.60	2.60
Pressure sensor IP65 G3/8 SEAFRONToewafv0c9q-01	1	24.90	24.90
Resistance 4700 Ω	9	0.17	1.53
Temperature sensor DS18B20	1	2.00	2.00
Waterproof housing	1	∼100	∼100

Electronics

ArduinoUNO Rev3 SMD is used as the microcontroller board that manages and initiates the electrical circuit. It is connected to an Adafruit Data Logging shield, which already includes an SD card for saving raw data and a Real Time Clock (RTC) to keep time. To increase temporal resolution, milliseconds from the start of the activation are stored in the output file. A 74HC4051 8-channel multiplexer is used to accommodate more analog sensors than supported by the ArduinoUNO alone, as explained below. The system operates using a 9 V battery for power supply. All the connections of the electrical circuit have been soldered on a third board. A picture of the electronics is shown in Fig. 1f, while the circuit diagram is shown in Fig. 2.

The primary sensor components of DISCO are LDRs. Light-dependent resistors are resistors whose resistance varies with irradiance within the spectrum centered on the visible range (which is why they are commonly called light-dependent resistors). Both upward-looking and downward-looking LDRs are installed to measure the decay profiles of downwelling and upwelling planar irradiance, respectively, and to estimate the corresponding attenuation coefficients K_d (downwelling) and K_u (upwelling). Specifically, their resistance increases with decreasing irradiance. Cadmium sulfide (CdS) LDRs of the NSL-19 M51 series from Luna Optoelectronics are used in this first version of the DISCO. They have a dimension of 4.1 mm × 4.1 mm, are 1.8 mm thick and provide a spectrally integrated response with a peak at 550 nm (i.e., in the center of the PAR range). A total of eight LDRs, four for each orientation, are installed to ensure redundancy in the measurements. To record voltage variations in the circuit resulting from changes in resistance of the LDR due to irradiance variation, each LDR is

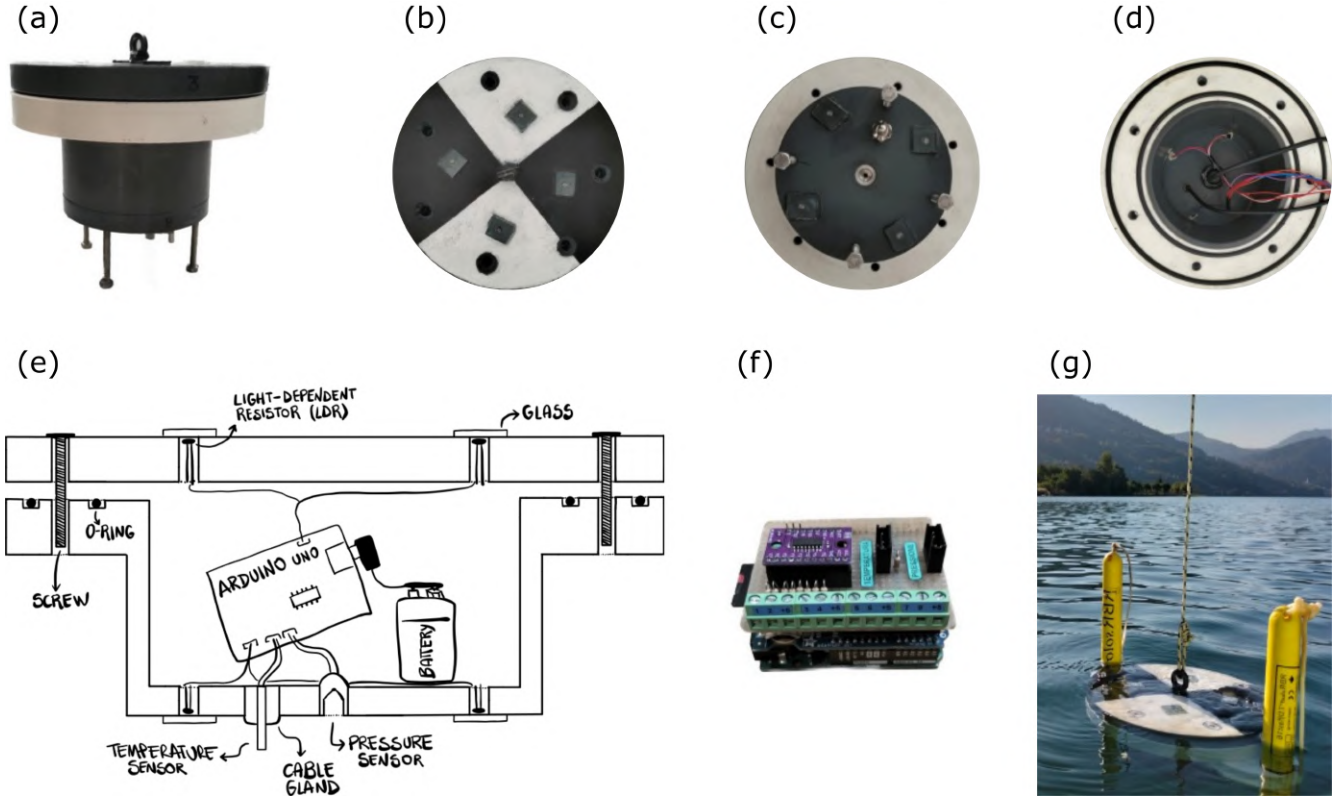

Fig. 1. Views of DISCO from different angles: (**a**) side view, (**b**) top view of the lid, (**c**) bottom view, (**d**) inside view, (**e**) schematic of DISCO, (**f**) electronics, and (**g**) DISCO deployed at Lake Serraia with the reference PAR, pressure and temperature sensors.

connected in series with a fixed reference resistor R_R of 4700 Ω in this case across an operating 5 V supply (*see* Fig. 2). This forms a voltage divider configuration where current flows through LDR first, then through the R_R, with the junction between them connected to an analog input pin of ArduinoUNO. The ArduinoUNO performs a 10-bit analog-to-digital conversion of the voltage at this junction, allowing for 2^{10} possible combinations. The resulting analog reading A ranges between 0 and 1023. Using the Ohm's law, the voltage at the junction (V_j) between the LDR and the R_R can be expressed as:

$$V_j = V_{in}\frac{R_R}{R_R + R_{LDR}} \tag{2}$$

where $V_{in} = 5$ V is the circuit voltage, and R_{LDR} is the resistance of the LDR. Rearranging the equation for R_{LDR}:

$$R_{LDR} = R_R\frac{V_{in} - V_j}{V_j} \tag{3}$$

Everything in this equation is known, since the voltage V_j is linked to the analog read A, recorded by the Arduino through the following linear relationship:

$$V_j = V_{in}\frac{A}{1023} \tag{4}$$

This configuration and this procedure allow the varying resistance of the LDR to be converted to a measure of irradiance by the calibration step described in the Sensors calibration and validation section. We note that since ArduinoUNO has six analog input pins, and each LDR requires one (in addition to those required by the RTC, multiplexer and pressure sensor, as shown in Fig. 2a), incorporating eight LDRs necessitates the inclusion of an 8-channel multiplexer for expansion. A simpler circuit can be constructed if the user is satisfied with using only three LDRs. In this case, the 8-channel multiplexer is unnecessary, and the available analog pins A0, A2, and A3 can be utilized for the LDRs (*see* Fig. 2b).

A pressure sensor continuously measures the depth of DISCO during profiling. The sensor mounted in this version of DISCO (model SEAFRONToewafv0c9q-01, waterproof IP65 G3/8) supports a maximum pressure of 2 bar, corresponding to approximately 20 m, which is appropriate for water clarity measurements in inland waters. The pressure sensor is connected to an analog input pin of ArduinoUNO (*see* Fig. 2). A linear relationship exists between the voltage V_P output from the pressure sensor and the pressure P. The voltage V_P is

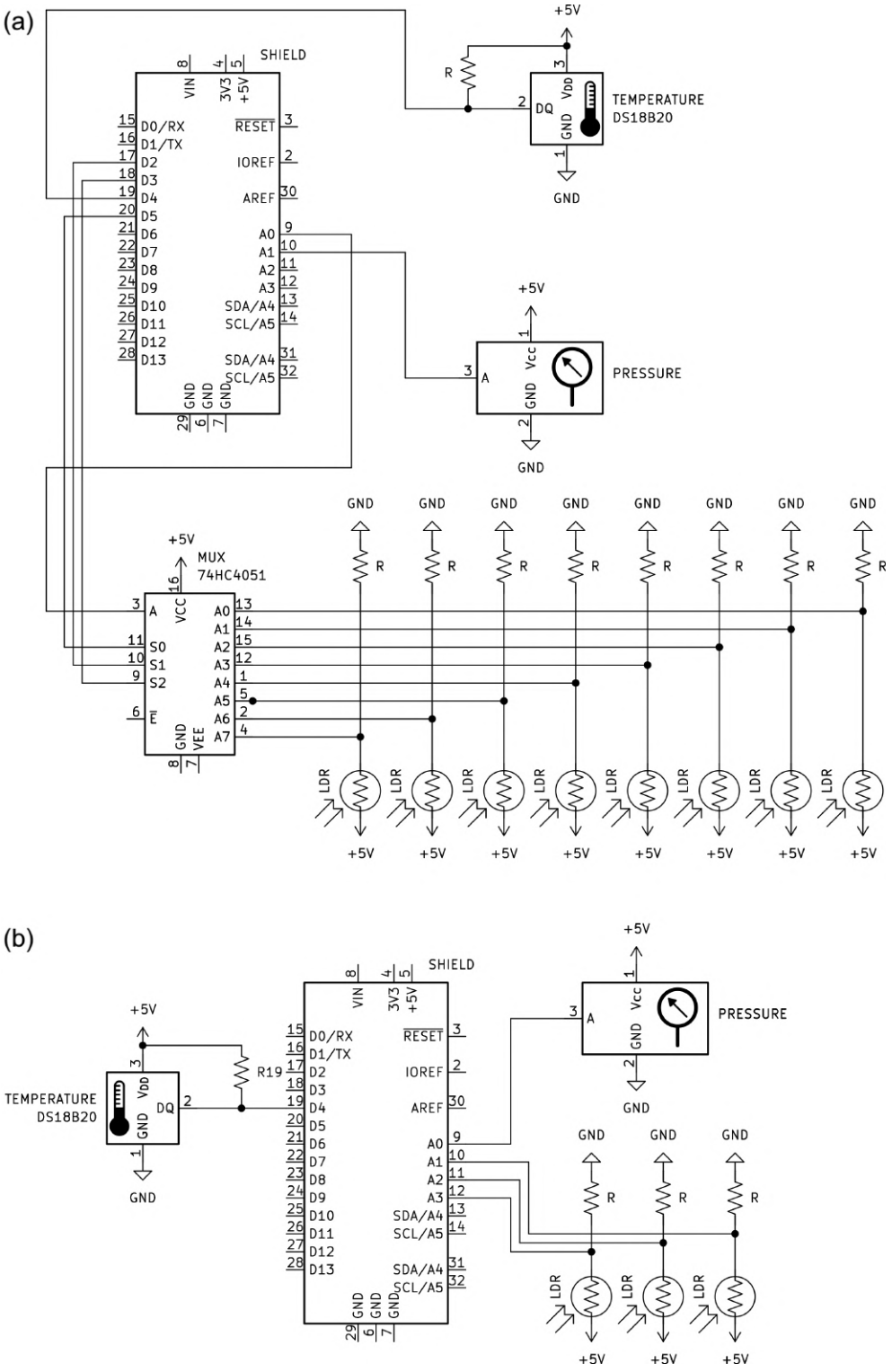

Fig. 2. Electrical schematic of DISCO in its full configuration (**a**), which integrates the Adafruit Data Logging shield (including the Real Time Clock, RTC, and the SD card) and the multiplexer (MUX) along with the irradiance (LDR), pressure and temperature sensors. The simplified version (**b**) without the MUX is also shown. The ArduinoUNO microcontroller is not shown in the figure as the Adafruit shield shares the same connection channels and is directly attached to the Arduino. The schematic was created using KiCad v8.0.6.

quantified using the same linear relationship as presented in Eq. 4, where A denotes the analog input from the sensor. According to the sensor specifications, a voltage range from 0.5 to 4.5 V corresponds to a pressure range from 0 to 2 bar, respectively. The pressure P (in bars) is therefore calculated as:

$$P = (V_P - V_{atm}) \frac{2\,\text{bar}}{4.5\,V - 0.5\,V} \tag{5}$$

where $V_{atm} = V_{in} \frac{A_{atm}}{1023}$ is the no-load output voltage, theoretically equal to 0.5 V, that is calibrated every time from the analog reading acquired when DISCO is out of the water before deployment, A_{atm}, to account for the atmospheric pressure, and $V_{in} = 5$ V. From Eq. 5 it is evident that the resolution of the pressure sensor is 2.4×10^{-3} bar, approximately equal to 2.5 cm, which suffices for the current application. Pressure sensors with a higher scale would yield to coarser resolutions, thereby limiting their suitability for this application. The pressure time series can be converted to the corresponding depth time series using the equation of state of water (either for saline or fresh water). Since the pressure sensor is mounted at the bottom of the PVC housing, it measures the depth for the downward-looking LDRs, while a fixed 12 cm adjustment is needed for the upward-looking LDRs installed in the DISCO lid (*see* section Waterproof housing for the dimensions of the waterproof housing).

A digital temperature sensor (DS18B20) is integrated into DISCO to measure this crucial water quality parameter. Positioned at the bottom of the profiling platform, it ensures that readings are taken in undisturbed conditions, unaffected by DISCO's wake. This sensor is connected to a digital pin of ArduinoUNO and directly provides water temperature measurements without the need for any conversion. To operate, the temperature sensor requires a resistor in series, which is fixed at 4700 Ω in this setup (*see* Fig. 2). Although the time response of the DS18B20 does not allow for capturing the fine structure of a temperature profile, its presence is still relevant for recording the background water temperature profile, which can be used to more accurately convert pressure into water depth and more completely characterize the water column.

The microcontroller is programmed with a script written in the Arduino IDE, and it operates at approximately 2 Hz. The output file obtained contains the raw data from the sensors, including analog readings from LDRs and pressure sensors, as well as temperature data from the DS18B20. Post-processing of the analog readings from LDRs and the pressure sensor is necessary using Eqs. 2–5 to obtain resistance and pressure values, respectively. The ArduinoUNO programming script and the script to convert to physical units are available at (Donini and Piccolroaz 2024). The list of sensors and electronic components used to assemble DISCO, along with their costs, is provided in Table 1.

Sensors calibration and validation

As explained in the previous section, the LDRs mounted on DISCO provide varying electrical resistance as a function of irradiance. To quantify the irradiance attenuation coefficients K_d and K_u using the LDRs, the electrical resistance must be calibrated against a reference radiometer to convert it into a PAR measure. We did this using the commercial cosine radiometer RBRsolo^{3}PAR, which provides a uniform response to light in the PAR spectral range between 400 nm and 700 nm. Photosynthetically active radiation is measured in μmol/m^2/s with a resolution of 0.001 μmol/m^2/s and an acquisition frequency up to 16 Hz.

In parallel, we used the two-channel logger RBRduet^{3}T.D as a reference to validate the low-cost depth and temperature sensors mounted on DISCO. The commercial logger provides accurate temperature and pressure measurements with a resolution of less than 5×10^{-5}°C for temperature and less than 1×10^{-3}% of the full scale for pressure (i.e., $< 1 \times 10^{-3}$ bar, equivalent to < 1 cm, in the case of the 100 bar maximum depth sensor used in this application).

The RBR probes were mounted on the side of DISCO (*see* Fig. 1f). Specifically, the RBR temperature and pressure probe was installed with the sensors positioned at the same level as the corresponding sensors mounted on the underside of the DISCO. The RBR PAR probe, on the other hand, was installed alternately with the PAR sensor positioned at the level of the upward- or downward-looking LDRs, aiming to fine-tune the calibration of both sets of LDRs. Several irradiance and temperature profiles were acquired under real lake conditions. Specifically, 51 vertical profiles (21 with the downward-looking RBR PAR and 30 with the upward-looking RBR PAR probe) were acquired in two mountain lakes in northern Italy: Lake Serraia, on three different days (6 Sept. 2023, 11 Oct. 2023, and 27 Oct. 2023), and Lake Caldonazzo, on two day (11 Oct. 2023 and 22 Jul. 2024). Lake Serraia (974 m a.s.l.) is a shallow eutrophic lake with periodic algal blooms. The average depth is 7 m while the maximum is 18 m, and the surface area is 0.45 km^2. Lake Caldonazzo (449 m a.s.l.) has an average depth of 26.5 m, a maximum depth of 49 m, and a surface area of 5.6 km ^{2}. Since 1989, it has undergone a process of re-oligotrophication due to a change in wastewater management (Flaim et al. 2016). The acquired profiles were used to calibrate the LDRs sensors, validate the pressure and temperature sensors, and test DISCO.

Concerning the validation of the LDRs, a linear relationship is found between LDR resistance (hereafter referred simply to as R) and PAR measured with the RBR PAR probe, on a bi-logarithmic scale (Fig. 3). Mathematically, this can be expressed as follows:

$$\ln(PAR) = -m_{calib} \cdot \ln(R) + q \tag{6}$$

where m_{calib} is the slope and q the intercept of the line. Every LDR must be calibrated separately, as they may exhibit slightly

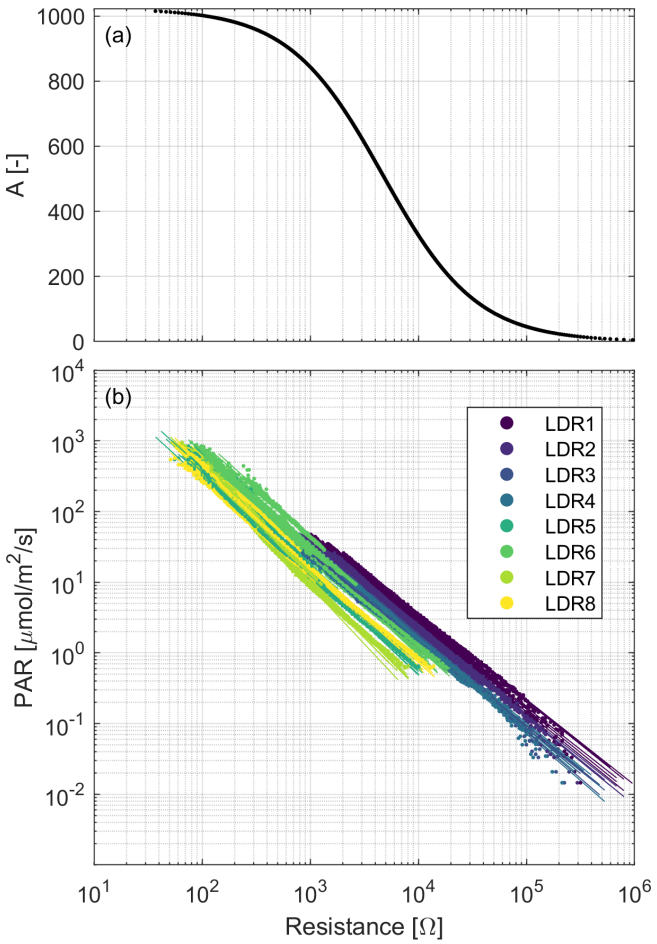

Fig. 3. Relationship between the LDR resistance (R) and (**a**) the analog reading (A) (semi-logarithmic scale) and (**b**) PAR measured by the RBR PAR probe (bi-logarithmic scale) for all the 51 acquired profiles. Different colors indicate different LDRs, with yellowish colors associated with upward-looking LDRs and bluish colors associated with downward-looking LDRs.

different light responses (i.e., m_{calib} and q values) due to variations in manufacturing and the presence of glass protection on DISCO. For each LDR, the slope m_{calib} was computed by fitting a linear model to each of the profiles for which reference RBR PAR data were available. The mean value of m_{calib} across these profiles was then calculated, and its uncertainty was assessed using the standard deviation (σ_{calib}) of the slope estimates. The standard deviation (σ_{calib}) is critical in assessing the uncertainty associated with the irradiance attenuation coefficient K using error propagation theory, as detailed in the following section. However, it is not necessary if the goal is solely to determine the expected value of K.

We note that the LDRs mounted in DISCO are housed under a protective glass cover, shielded from harsh environmental conditions. This setup contributes to the stability of the LDRs and mitigates aging effects. Therefore, periodic calibration of the LDRs may be sufficient.

Evaluation of the irradiance attenuation coefficient *K*

The logarithm of the Beer–Bouguer–Lambert law in Eq. 1 reads:

$$\ln(PAR) = -Kz + \ln(PAR_0) \tag{7}$$

where the generic irradiance I is replaced by PAR, as PAR was measured with the RBRsolo^{3}PAR in this study. The empirical estimate of the irradiance attenuation coefficient K can be easily determined by linear fitting the PAR-z measured data according to the above equation. For each measured profile, we can therefore determine the corresponding irradiance attenuation coefficient K, here referred to as K_{RBR} to indicate that it is determined using the PAR reference data. The uncertainty associated with K_{RBR} can be assessed using the standard deviation (σ_{RBR}) of the slope estimate obtained from the linear fit.

A similar procedure can be used to quantify K based on the LDRs. By substituting the expression for $\ln(PAR)$ in terms of $\ln(R)$ from Eq. 6 into the logarithm of the Beer–Bouguer–Lambert law provided in Eq. 7, we derive the following equation, which describes the electrical resistance profile associated with the existing PAR profile:

$$\ln(R) = \frac{Kz}{m_{calib}} + \ln(R_0) \tag{8}$$

where, according to the notation used in Eq. 1, R_0 is the electrical resistance value associated with PAR at the surface (i.e., PAR_0) and its logarithm is equal to $\ln(R_0) = \frac{q - \ln(PAR_0)}{m_{calib}}$. This equation links the irradiance attenuation coefficient K with the LDR measurements, through the calibration coefficient m_{calib}. In other words, along a water column with constant water clarity, any LDR would measure an electrical resistance profile consistent with this equation, which is a linear function in the $\ln(R)$-z plane. Thus, performing the linear regression on the measured $\ln(R)$-z data allows to quantify the slope of this line, which we call m_R and that according to Eq. 8 is $m_R = \frac{K}{m_{calib}}$. The evaluation of the irradiance attenuation coefficient K follows directly as:

$$K_{LDR} = m_R \cdot m_{calib} \tag{9}$$

where the subscript indicates that it is determined using the LDR data.

For each vertical profile, the uncertainty associated with m_R can be assessed using the standard deviation (σ_R) of the slope estimate obtained from the linear fit, exactly as done for the case of the PAR reference data discussed at the beginning of this section. This quantity can be combined with the uncertainty associated with m_{calib} (i.e., σ_{calib}) to assess the overall uncertainty in the estimate of K_{LDR} for each vertical profile. By assuming that m_{calib} and m_R are independent, according to

error propagation theory of Eq. 9, the standard deviation of K_{LDR} is given by:

$$\sigma_{LDR} = K_{LDR}\sqrt{\left(\frac{\sigma_{calib}}{m_{calib}}\right)^2 + \left(\frac{\sigma_R}{m_R}\right)^2} \tag{10}$$

so that the light attenuation is $K_{LDR} \pm \sigma_{LDR}$ and this will be compared to the reference value $K_{RBR} \pm \sigma_{RBR}$. We note that the intercept $\ln(R_0)$ in Eq. 8, hence the parameter q in Eq. 6, is not needed for the evaluation of K_{LDR} and its uncertainty. However, it is required if the goal is to convert R into an absolute measure of PAR.

For simplicity, the subscripts d and u are omitted when referring to K in the rest of the manuscript, depending on whether we are talking about downwelling or upwelling light attenuation. The results are presented separately according to the sensor orientation.

Deployment and processing procedure

The procedural steps used to pre-process and analyze the acquired irradiance profiles and to evaluate the expected value of K and its uncertainty are outlined below. The same approach is used to identify and pre-process the RBR reference PAR data.

1. Deploy DISCO to acquire one or more profiles (suggested profiling speed between 0.1 and 1.0 m/s).
2. Read the SD card where the data is saved and convert the analog readings (A) to obtain electrical resistance and pressure using Eqs. 2–5.
3. Use the pressure time series to calculate the profiling speed $v = \frac{dP}{dt}$ in dbar/s (or, analogously, use the depth time series to get $v = \frac{dz}{dt}$ in m/s, once presssure is converted into depth).
4. Identify the downward vertical profiles from the velocity time series. Specifically, a profile begins when the velocity threshold of 5×10^{-3} dbar/s and the minimum pressure of 0.1 dbar are exceeded, with the velocity sign indicating the profiling direction. Segment the time series at the vertical profiles and save the LDR resistance, pressure, and temperature data for subsequent analysis. It is important to note that only downward profiles are analyzed in this study to minimize potential disturbances caused by the wake generated by the moving platform. Upward profiles can be used as well, but it is advisable to wait a reasonable amount of time after the DISCO has reached its lowest point before starting recovery.
5. Perform a quality check on each resistance profile to identify and remove any boundary contamination caused, for example, by light scattering and reflections near the surface and close to the bottom (if reached by DISCO) or wave focusing and defocusing due to surface waves (Gege and Pinnel 2011). Specifically, the profile is divided into bins of a selected size (e.g., 1 m), 50% overlapped to increase the resolution of the quality check analysis (a standard also in the context of turbulence measurements, [Sebastiano Piccolroaz et al. 2021]). The vertical profile of the natural logarithm of the data in each bin is linearly detrended, and residuals exceeding a user-defined threshold are removed. In this analysis, a threshold of 0.1 is used, corresponding to the removal of all residuals where:

$$\epsilon = \ln(R) - \ln(R_{\text{fit}}) = \ln\left(\frac{R}{R_{\text{fit}}}\right) < 0.1 \tag{11}$$

   where $\ln(R_{fit})$ denotes the fitted values in the logarithmic scale. In bins where the linear fit is poor ($R^2 < 0.5$) or statistically non-significant (p-value > 0.1), indicating large scatter, all values are removed.
6. Interpolate each cleaned resistance profile along depth in the semi-logarithmic plane $\ln(R) - z$ using a linear fit to determine its slope m_R and its standard deviation σ_R (*see* section Evaluation of the irradiance attenuation coefficient K).
7. Given m_{calib} and m_R, along with their respective standard deviations, use Eqs. 9 and 10 to determine the expected value of K and its standard deviation, respectively.

Assessment

In this section, we provide an overview of DISCO's performance against the commercial PAR, pressure, and temperature sensors used as references. The analysis is carried out considering the 51 vertical profiles acquired in two different lakes and in different time periods, as described in the Sensors calibration and validation section and summarized in Table 2.

Validation of the pressure and temperature sensors

First, we start by the validation of the low-cost pressure and temperature sensors mounted on DISCO. Fig. 4 shows the comparison between the pressure (Fig. 4a) and water temperature (Fig. 4b) data obtained with the sensors mounted on DISCO and the reference values measured with the

Table 2. Summary of the vertical profiles performed, indicating the total number of profiles (n_t), the number of profiles acquired with the commercial RBR instrument positioned up (n_u) and down (n_d). The Secchi disk depth (z_{SD}) measured by the operator using DISCO is also reported.

Lake	Date	n_t	n_u	n_d	z_{SD}
Serraia	6 Sep 23	7	4	3	3.10
Serraia	11 Oct 23 (AM)	10	5	5	3.20
Serraia	11 Oct 23 (PM)	18	9	9	3.20
Caldonazzo	11 Oct 23	5	5	0	5.30
Serraia	27 Oct 23	7	4	3	2.10
Caldonazzo	22 Jul 24	4	4	0	3.00
Total		**51**	**31**	**20**	

commercial probe RBRsolo^{3}T.D. Overall (i.e., considering all the 51 available profiles, *see* Table 2), the Root Mean Square Error (RMSE) for the pressure is 0.03 dbar (corresponding to approximately 3 cm) while for water temperature it is 0.21°C (we note that the temperature data from the field campaign done on July 2024 are not included here, due to malfunctioning of the temperature sensor installed on DISCO). As for the pressure, we bias corrected the DISCO time series against the reference time series by removing the average difference between the two, calculated for each profile separately. In this way, we accounted for possible systematic difference between the two time series arising from slight disalignment between the two pressure sensors. The RMSE shown above can therefore be interpreted as resulting from the different resolution of the two sensors. Indeed, a RMSE = 0.03 dbar is consistent with the resolution of the pressure sensor mounted on DISCO (i.e., approximately = 0.024 dbar).

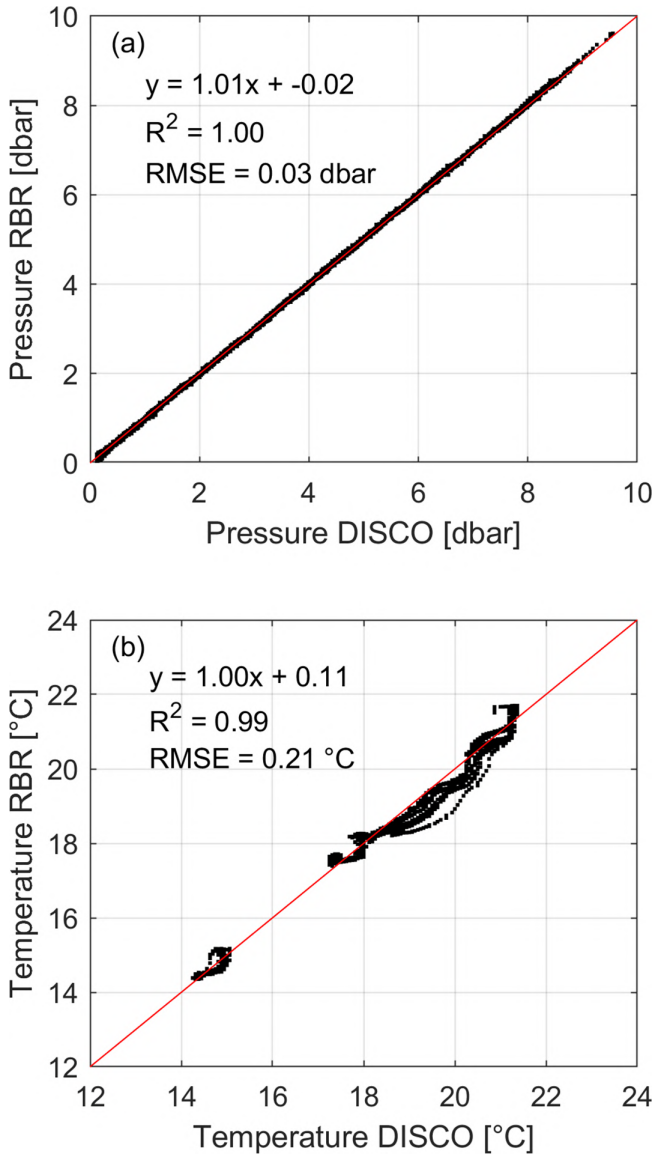

Fig. 4. Validation of the low-cost pressure and temperature sensors mounted on DISCO against the reference values obtained with the commercial probe RBRsolo^{3}T.D: (**a**) pressure and (**b**) water temperature. The data acquired by DISCO are plotted on the x-axis, while the reference values are plotted on the y-axis.

Calibration of the light-dependent resistors

The calibration of the upward- and downward-looking LDRs is carried out considering the subset of profiles for which reference PAR data, acquired with the RBRsolo^{3}PAR, are available and oriented in the same direction as the LDRs, that is, a total of 31 profiles for the upward-looking LDRs and of 20 for the downward-looking LDRs (*see* Table 2). Specifically, the reference PAR data and the electrical resistance data are linearly fitted in a bi-logarithmic plane to determine the calibration parameter m_{calib} and its variance σ_{calib}, as described in the Sensors calibration and validation section and shown in Fig. 3b. Before fitting, both the types of data are first denoised as described in the Deployment and processing procedure section to account for possible light scattering and reflections near the surface and near the bottom (i.e., the same procedure described for resistance R are applied to the reference RBR PAR data). This cleaning procedure also takes into account possible disturbances caused by the presence of submerged macrophyte vegetation in shallow conditions. As might be expected, downwelling irradiance (measured by both upward-looking LDRs and the RBR PAR probe) shows higher scattering close to the surface, while upwelling irradiance has a higher scattering near the bottom. This is summarized in Fig. 5, which shows the probability density distribution of the residual ϵ defined in Eq. 11 along depth (normalized relative to the maximum for each profile separately), for the upward-looking and downward-looking RBR PAR probe and LDRs. The majority of the data is well below the $\epsilon = 0.1$ threshold (bluish colors), and the above threshold values are found primarily for downwelling irradiance in both upward-looking sensors. Above threshold values are found to a lesser extent in the upwelling irradiance data, especially for the downward-looking RBR PAR probe, while they are minimal for the downward-looking LDRs. In general, in cases where high scattering is expected throughout the water column (e.g., in shallow lakes), it is recommended to take multiple profiles and analyze their average, possibly relaxing the quality checks to avoid filtering out too much data.

Remarkably, after denoising of the signal, the PAR-resistance relationship slightly deviates from linear for high ($> 10^2 \mu$mol/m^2/s) and, more evident, for low ($< 10^{-1} \mu$mol/m^2/s) PAR values, as evident in Fig. 3b. While the above-mentioned boundary disturbances may still have some residual effect after the cleaning procedure, the main reason in this case is associated with the saturation of the analog reading: where in these regions small changes in the analog

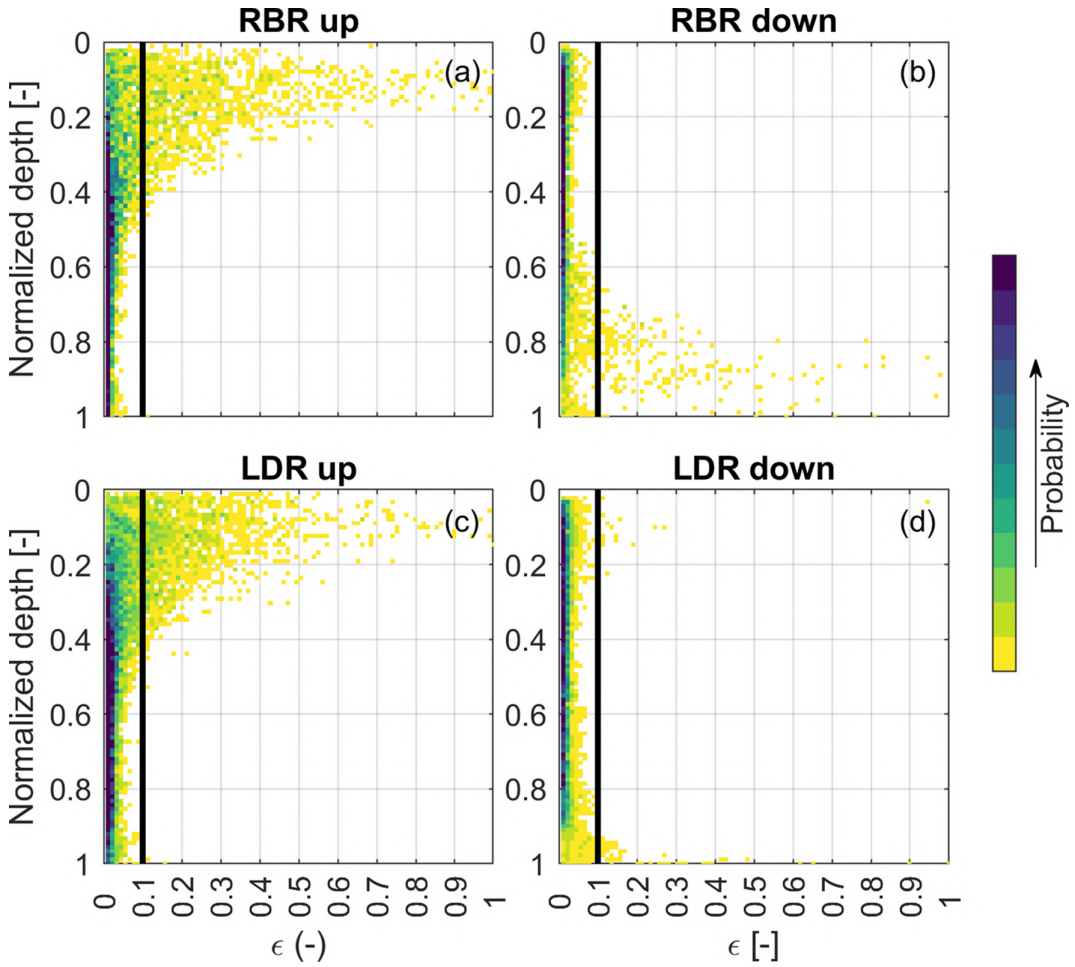

Fig. 5. Heatmap plots showing the probability density distribution (indicated by the color scale) of the residual ϵ defined in Eq. 11 for (**a**) upward-looking and (**b**) downward-looking RBR PAR probe and for (**c**) upward-looking and (**d**) downward-looking LDRs, along depth (normalized relative to the maximum for each profile separately). The black vertical line indicates the threshold used to discard noisy data.

reading correspond to a large change in resistance (*see* Fig. 3a). The effect is anyway mild, especially at the surface, and does not preclude the identification of robust and statistically significant linear fits between the logarithms of PAR and resistance (R^2 always >0.99 and p-value always $\ll 0.01$). The distribution of the m_{calib} parameters obtained from this linear fit is shown in Fig. 6 for each LDR separately. From these distributions, the expected values and associated uncertainty in m_{calib} are calculated as the mean and the standard deviation of each distribution, which are summarized in Table 3.

Finally, Fig. 7a shows the heatmap scatterplot between PAR as measured by the reference RBR probe and PAR as obtained by converting the electrical resistance measured by the LDRs by implementing Eq. 6 with the average values of m_{calib} and q for each LDR. The bulk of the data (bluish color) lies well on the 1 : 1 line over a wide range of PAR values, indicating a robust conversion from R to PAR, as confirmed by an RMSE of 26 μmol/m^2/s. Figure 7b illustrates that the percentage error of PAR DISCO relative to PAR RBR is generally moderate across the wide range of variability, limited within $\pm 25\%$ and with local increases at the extremes. These increases, limited to about 100%, are reasonable given the large range spanned by the data.

Performance of DISCO in assessing the irradiance attenuation coefficient *K*

The performance of DISCO in assessing the irradiance attenuation coefficient K is evaluated by comparing the coefficients obtained from the commercial instrument, K_{RBR}, and the LDRs mounted on DISCO, K_{LDR}, computed based on the available vertical profiles (Table 2) according to the procedure described in the Evaluation of the irradiance attenuation coefficient K section. For a fair comparison, the irradiance attenuation coefficients are only calculated taking into account depths where both the RBR reference PAR sensor data and LDRs are available (for each profile and LDRs separately).

The comparison is shown in Fig. 8, separately for the upward-looking and downward-looking sensors, using

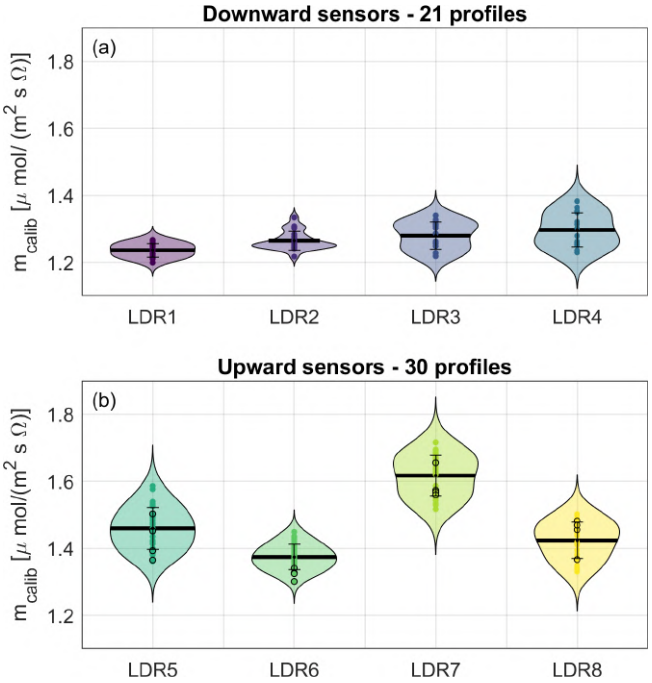

Fig. 6. Violin plots showing the distribution of m_{calib} for each LDR, including both (**a**) downward-looking (LDR1-4) and (**b**) upward-looking (LDR5-8) sensors, evaluated across all available profiles. The black line represents the mean, the error bar the standard deviation, and the dots the individual values (dots with a black border refer to measurements taken on 22 July 2024). The figure has been generated using exttt{violin.m} provided by Hoffmann (2015).

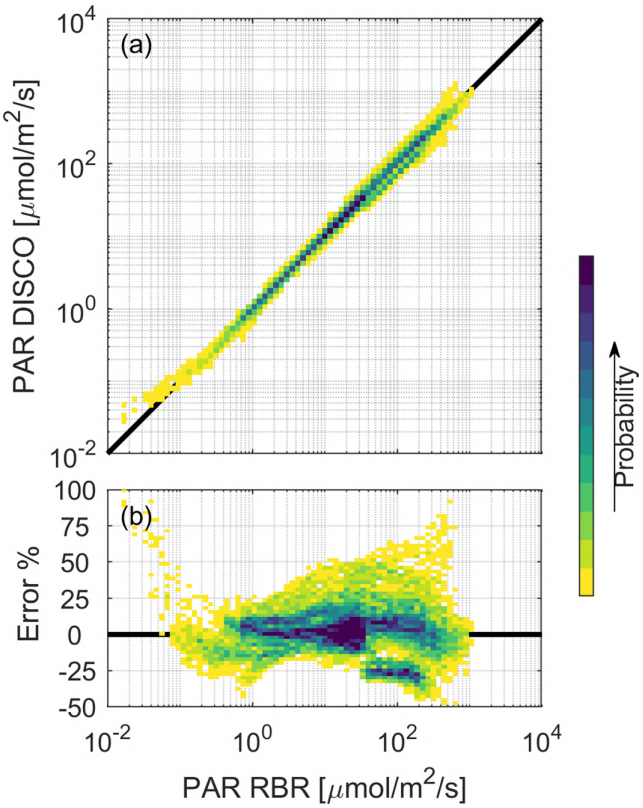

Fig. 7. Heatmap scatterplot comparing PAR values: (**a**) PAR as measured by the reference RBR probe (y axis) vs. PAR values obtained using Eq. 6 with average values of m_{calib} and q for each LDR (x axis). The black line represents the 1 : 1 line. (**b**) Percentage error of PAR DISCO relative to PAR RBR as a function of PAR RBR. The probability density of data points is indicated by the heatmap color scale.

different colors for the different LDRs and different symbols for the different field campaigns. The uncertainty associated with K_{LDR} is larger than that associated with K_{RBR}, as expected, due to the contribution of σ_{calib} in Eq. 10 but still acceptably small: $\sigma_{LDR} = 0.023 \pm 0.009$ m^{-1} to compare with $\sigma_{RBR} = 0.004 \pm 0.005$ m^{-1}. The data are well aligned along the 1 : 1 line and contained within the $\pm 10\%$ interval (dashed lines), indicating good agreement between DISCO and the reference PAR sensor across a relatively wide range of values: 0.3–1.1 m^{-1} for K_d (i.e., upward-looking sensors) and 0.6–0.9 m^{-1} for K_u (i.e., downward-looking sensors). We note that in the latter case, the range is smaller because the downward-looking reference PAR data were not available in the case of Lake Caldonazzo due to noisy data associated with scattering from the bottom in October 2023 and harsh wind conditions that prevented the acquisition of further data in July 2024.

Table 3. Summary statistics of m_{calib} and σ_{calib} for each LDR.

LDRs ID	m_{calib} [μmol/(m^2 s Ω)]	σ_{calib} [μmol/(m^2 s Ω)]
LDR1	1.237	0.020
LDR2	1.265	0.028
LDR3	1.280	0.041
LDR4	1.297	0.051
LDR5	1.460	0.062
LDR6	1.374	0.038
LDR7	1.617	0.061
LDR8	1.424	0.054

Finally, it is important to note that the values calculated here represent the mean attenuation coefficient along the water column, chosen as a reasonable parameter for validating DISCO. On 6 September 2023, Lake Serraia experienced a massive algal bloom (*Microcystis aeruginosa* and *Woronichinia naegeliana*), resulting in two distinct slopes in the irradiance profiles. Under these conditions, interpolating a single line over the entire depth is not practically representative, but it remains valid for validation purposes. The deviation of some points from the 1 : 1 line beyond the 10 % interval range in Fig. 8b can be attributed to this effect. In such cases, where varying attenuation coefficients are observed along the water column, we recommend dividing the column into distinct layers and calculating separate attenuation coefficients for each layer.

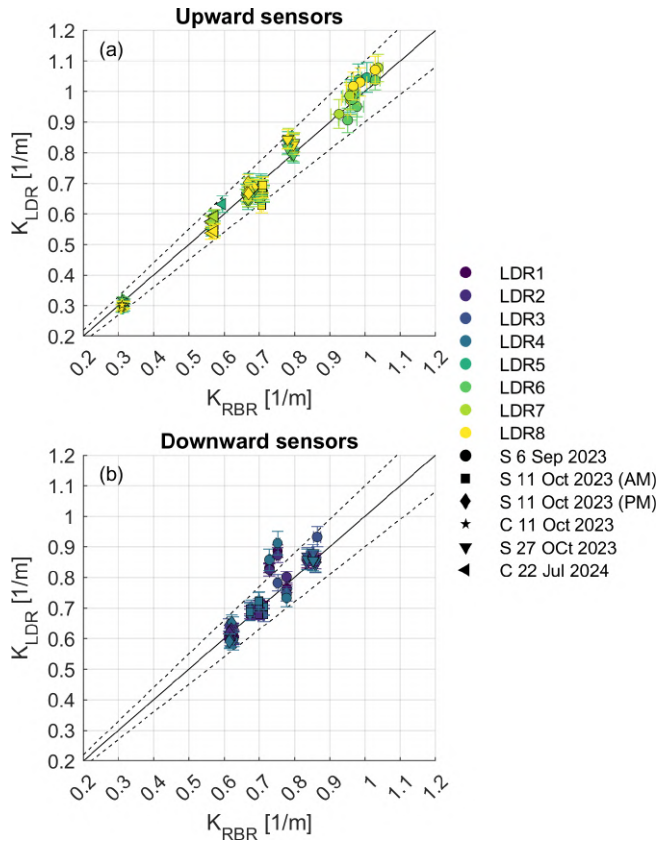

Fig. 8. Comparison of the attenuation coefficients obtained from the commercial reference instrument (K_{RBR}) and DISCO (K_{LDR}), for (**a**) upward-looking sensors and (**b**) downward-looking sensors. The uncertainties (σ_{RBR} and σ_{LDR}) are also shown as error bars and the $\pm 10\%$ limits are shown as dashed lines around the 1 : 1 continuous line. Different colors refer to different LDRs and different symbols to different field campaigns.

Discussion

The development of DIY devices (Bardaji et al. 2016; Rodero et al. 2022; Brewin et al. 2024) and the use of cheap sensors (Scordo et al. 2024) for measuring irradiance profiles and estimating the corresponding attenuation coefficients in water bodies has recently attracted renewed interest from the scientific community. In this contribution, we presented DISCO, an easy to build and cheap ($\sim$180 €) DIY instrument for water clarity observations. Two common metrics used to monitor water clarity are the vertical PAR attenuation coefficient (K) and the Secchi disk depth (z_{SD}). DISCO combines these in a single instrument by incorporating irradiance detectors (photoresistors, LDRs) and pressure sensors into a structure with the appearance of the standard Secchi disk for limnological applications. Light-dependent resistors are mounted both upward- and downward-looking to measure the downwelling and upwelling irradiance attenuation coefficients, respectively. Four LDRs are mounted in each orientation to ensure redundancy of measurements. A temperature sensor is also installed to record the water temperature.

Once the LDRs are calibrated against a reference radiometer (e.g., a commercial PAR sensor, as in this case), DISCO offers a cheaper alternative to the use of expensive radiometers to measure irradiance profiles (*see* Fig. 7) and irradiance attenuation coefficients (*see* Fig. 8). Thanks to the temporal stability of the LDRs, further guaranteed by the fact that they are housed in an isolated cavity under a protective glass, the calibration of the LDRs to convert electrical resistance into irradiance is an operation that can be carried out occasionally. This is confirmed by the results in terms of m_{calib} obtained in July 2024, which are consistent with those obtained in September–October 2023 (*see* Fig. 6).

Each LDR has a slightly different m_{calib} due to variations in the sensor itself and the protective glass (*see* Fig. 6). In addition, the value of the calibration parameter m_{calib} differs between the downward-looking sensors ($m_{calib} \sim 1.27$ μmol/(m^2 s Ω)) and upward-looking sensors ($m_{calib} \sim 1.47$ μmol/(m^2 s Ω)), which may be due to spectral differences in the light source in the two cases. In fact, the LDRs, with their spectrally integrated response peaking at 550 nm, and the reference PAR probe, with a cosine-corrected, uniform spectral response integrated between 400 and 700 nm, have a different spectral sensitivity (Kuroiwa et al. 1983), which is embedded in the m_{calib} and q parameters during calibration. It should be noted, however, that if the water composition (hence the underwater light spectrum) changes significantly from that in which the calibration was performed, m_{calib} and q may also change somewhat. However, in the present study, irradiance profiles were carried out at different times of the year and in two different lakes, which resulted in fairly stable values of m_{calib} (and q), suggesting reasonable reliability of the proposed methodology in "standard" lake waters across seasons, phytoplankton concentrations and species, and water clarity conditions. The standard deviation of the calibration parameter is slightly larger for the upward-looking sensors, due to the larger scatter of the data near the surface (*see* Fig. 5), which may affect the fitting of Eq. 6 even after cleaning the signal. Overall, the results indicate that DISCO can be used to estimate both K_d and K_u with an error of less than 10% compared to the reference PAR probe, across a relatively wide range of values (*see* Fig. 8). Also, the uncertainty associated with the estimation of the irradiance attenuation coefficients, primarily due to the uncertainty associated with m_{calib} m is limited ($\sigma_{LDR} = 0.023 \pm 0.009$ m^{-1}) and does not preclude reliable measurements.

Building DISCO does not require any special knowledge of electronics, which makes it accessible for autonomous preparation by anyone and therefore potentially widely available. Unlike the solution proposed by Brewin et al. (2024), where the electronics are encapsulated in epoxy resin, DISCO allows access to the electronics, making it easy to replace components and perform upgrades. Improving DISCO would

enhance its usability and enrich the data, but it would come at the cost of simplicity. Users must therefore match their specific needs with their electronics background and the facilities to which they have access.

Comments and recommendations

To address the need for affordable and reliable optical sensing solutions as an alternative to expensive commercial sensors, we have introduced DISCO, a DIY optical profiling system. DISCO has good accuracy and precision, comparable to commercial alternatives, but is more cost-effective and its realization is accessible, even for people with limited electronics background. This last point was the leitmotif of the project, which aimed to make the device potentially widely available and realizable for people all over the world, promoting participatory science, and supporting education and outreach efforts. In addition, DISCO has the appearance of a Secchi disk, allowing the standard Secchi disk measurement to be retained, providing continuity to existing databases, often dating back several decades, while adding an objective estimate of the attenuation coefficient K. All the scripts for programming the microcontroller and for post-processing the data, as well as the data themselves, are provided in order to encourage the widest and easiest use of the instrument and to allow continuous improvement by those who decide to develop DISCO or simply to use the processing scripts. In this last respect, the post-processing script (in particular the cleaning algorithm) can be useful for estimating the irradiance attenuation coefficient, regardless of the type of sensor or device used to acquire the data.

Acknowledgments

We thank Lorenzo Forti (Hydraulics Laboratory of the University of Trento) for the support in building the housing of DISCO, and Claudio Salomon (Electronics and Design Service of the University of Trento) for the advice on the design of the electronics. We acknowledge the Italian Ministry of Universities and Research (MUR), in the framework of the project DICAM-EXC (Departments of Excellence 2023–2027, Grant L232/2016). Open access publishing facilitated by University of Trento, as part of the Wiley - CRUI-CARE agreement.

Conflicts of Interest

None declared.

References

Aas, E., J. Høkedal, and K. Sørensen. 2014. "Secchi Depth in the Oslofjord-Skagerrak Area: Theory, Experiments and Relationships to Other Quantities." *Ocean Science* 10: 177–199. https://doi.org/10.5194/os-10-177-2014.

Bardaji, R., A. M. Sánchez, C. Simon, M. R. Wernand, and J. Piera. 2016. "Estimating the Underwater Diffuse Attenuation Coefficient With a Low-Cost Instrument: The KdUINO DIY Buoy." *Sensors* 16, no. 3: 373. https://doi.org/10.3390/s16030373.

Beer. 1852. "Bestimmung Der Absorption Des Rothen Lichts in Farbigen Flüssigkeiten." *Annalen der Physik* 162: 78–88. https://doi.org/10.1002/andp.18521620505.

Bouffard, D., and A. Wüest. 2019. "Annual Review of Fluid Mechanics Convection in Lakes." *Annual Review of Fluid Mechanics* 51: 189–215. https://doi.org/10.1146/annurev-fluid-010518.

Bouffard, D., G. Zdorovennova, and S. Bogdanov. 2019. "Under-Ice Convection Dynamics in a Boreal Lake." *Inland Waters* 9: 142–161. https://doi.org/10.1080/20442041.2018.1533356.

Brewin, R. J. W., T. G. Brewin, P. J. Bresnahan, et al. 2024. "Lab on a Secchi Disk: A Prototype Open-Source Profiling Package for Low-Cost Monitoring in Aquatic Environments." *Limnology and Oceanography: Methods* 22: 507–526. https://doi.org/10.1002/lom3.10624.

Brewin, R. J. W., T. G. Brewin, J. Phillips, et al. 2019. "A Printable Device for Measuring Clarity and Colour in Lake and Nearshore Waters." *Sensors (Basel, Switzerland)* 19, no. 4: 936. https://doi.org/10.3390/s19040936.

Cristofor, S., A. Vadineanu, G. Ignat, and C. Ciubuc. 1994. "Factors Affecting Light Penetration in Shallow Lakes." *Hydrobiologia* 275: 493–498. https://doi.org/10.1007/BF00026737.

Donini, G., and S. Piccolroaz. 2024. "Supporting Material—DISCO: A Low-Cost Device-Instrumented Secchi Disk for Water Clarity Observations." *Zenodo*. https://doi.org/10.5281/zenodo.14419602.

Dresti, C., M. Rogora, and A. Fenocchi. 2023. "Hypolimnetic Oxygen Depletion in a Deep Oligomictic Lake Under Climate Change." *Aquatic Sciences* 85, no. 1: 4. https://doi.org/10.1007/s00027-022-00902-2.

Flaim, G., E. Eccel, A. Zeileis, G. Toller, L. Cerasino, and U. Obertegger. 2016. "Effects of Re-Oligotrophication and Climate Change on Lake Thermal Structure." *Freshwater Biology* 61: 1802–1814. https://doi.org/10.1111/fwb.12819.

Gege, P., and N. Pinnel. 2011. "Sources of Variance of Downwelling Irradiance in Water." *Applied Optics* 50: 2192–2203. https://doi.org/10.1364/AO.50.002192.

Giardino, C., M. Pepe, P. A. Brivio, P. Ghezzi, and E. Zilioli. 2001. "Detecting Chlorophyll, Secchi Disk Depth and Surface Temperature in a Sub-Alpine Lake Using Landsat Imagery." *Science of the Total Environment* 268: 19–29. https://doi.org/10.1016/S0048-9697(00)00692-6.

Heiskanen, J. J., I. Mammarella, and A. Ojala. 2015. "Effects of Water Clarity on Lake Stratification and Lake-Atmosphere Heat Exchange." *Journal of Geophysical Research-Atmospheres* 120: 7412–7428. https://doi.org/10.1002/2014JD022938.

Hocking, G. C., and M. Straškraba. 1999. "The Effect of Light Extinction on Thermal Stratification in Reservoirs and Lakes." *International Review of Hydrobiology* 84: 535–556. https://doi.org/10.1002/iroh.199900046.

Hoffmann, H. 2015. Violin.m—Simple Violin Plot Using MATLAB Default Kernel Density Estimation.

Houser, J. N. 2006. "Water Color Affects the Stratification, Surface Temperature, Heat Content, and Mean Epilimnetic Irradiance of Small Lakes." *Canadian Journal of Fisheries and Aquatic Sciences* 63: 2447–2455. https://doi.org/10.1139/f06-131.

Kirk, J. T. O. 1977. "Use of a Quanta Meter to Measure Attenuation and Underwater Reflectance of Photosynthetically Active Radiation in some Inland and Coastal South-Eastern Australian Waters." *Australian Journal of Marine & Freshwater Research* 28: 9–22. https://doi.org/10.1071/MF9770009.

Kirk, J. T. O. 2010. Light and Photosynthesis in Aquatic Ecosystems. 3rd ed. Cambridge: Cambridge University Press.

Kuroiwa, S., T. Yukimura, and S. Takami. 1983. "Comparative Measurements of Underwater Irradiance in Illuminance, Quanta and Energy in Lake Biwa." *Japanese Journal of Limnology (Rikusuigaku Zasshi)* 44: 47–58. https://doi.org/10.3739/rikusui.44.47.

Lee, Z., S. Shang, C. Hu, et al. 2015. "Secchi Disk Depth: A New Theory and Mechanistic Model for Underwater Visibility." *Remote Sensing of Environment* 169: 139–149. https://doi.org/10.1016/j.rse.2015.08.002.

Lehmann, M. K., D. Gurlin, N. Pahlevan, et al. 2023. "GLORIA—A Globally Representative Hyperspectral In Situ Dataset for Optical Sensing of Water Quality." *Scientific Data* 10: 100. https://doi.org/10.1038/s41597-023-01973-y.

Lin, H. C., C. Y. Chiu, J. W. Tsai, W. C. Liu, K. Tada, and K. Nakayama. 2021. "Influence of Thermal Stratification on Seasonal Net Ecosystem Production and Dissolved Inorganic Carbon in a Shallow Subtropical Lake." *Journal of Geophysical Research: Biogeosciences* 126: e2020JG005907. https://doi.org/10.1029/2020JG005907.

Liu, M., Y. Zhang, Y. Zhou, K. Shi, G. Zhu, and X. Sun. 2022. "Thermal Structure Controlled by Morphometry and Light Attenuation Across Subtropical Reservoirs." *Hydrological Processes* 36: e14502. https://doi.org/10.1002/hyp.14502.

López Moreira, G. A., M. Toffolon, and F. Hölker. 2021. "Hitting the Sweet Spot of Complexity: Reasons Why the Development of New Custom-Tailored Models Is Still Warranted and Should Be Encouraged in Aquatic Sciences." *Journal of Limnology* 80: 2035. https://doi.org/10.4081/jlimnol.2021.2035.

Markelov, I., R. M. Couture, R. Fischer, S. Haande, and P. Van Cappellen. 2019. "Coupling Water Column and Sediment Biogeochemical Dynamics: Modeling Internal Phosphorus Loading, Climate Change Responses, and Mitigation Measures in Lake Vansjø, Norway." *Journal of Geophysical Research: Biogeosciences* 124: 3847–3866. https://doi.org/10.1029/2019JG005254.

Meyer, M. F., S. N. Topp, and T. V. King. 2024. "National-Scale Remotely Sensed Lake Trophic State From 1984 through 2020." *Scientific Data* 11, no. 1: 77. https://doi.org/10.1038/s41597-024-02921-0.

Nava, V., S. Chandra, J. Aherne, et al. 2023. "Plastic Debris in Lakes and Reservoirs." *Nature* 619: 317–322. https://doi.org/10.1038/s41586-023-06168-4.

Persson, I., and I. D. Jones. 2008. "The Effect of Water Colour on Lake Hydrodynamics: A Modelling Study." *Freshwater Biology* 53: 2345–2355. https://doi.org/10.1111/j.1365-2427.2008.02049.x.

Piccolroaz, S., B. Fernández-Castro, M. Toffolon, and H. A. Dijkstra. 2021. "A Multi-Site, Year-Round Turbulence Microstructure Atlas for the Deep Perialpine Lake Garda." *Scientific Data* 8: 188. https://doi.org/10.1038/s41597-021-00965-0.

Piccolroaz, S., S. Zhu, and R. Ladwig. 2024. "Lake Water Temperature Modeling in an Era of Climate Change: Data Sources, Models, and Future Prospects." *Reviews of Geophysics* 62, no. 1: e2023RG000816. https://doi.org/10.1029/2023RG000816.

Pilla, R. M., and R. M. Couture. 2021. "Attenuation of Photosynthetically Active Radiation and Ultraviolet Radiation in Response to Changing Dissolved Organic Carbon in Browning Lakes: Modeling and Parametrization." *Limnology and Oceanography* 66: 2278–2289. https://doi.org/10.1002/lno.11753.

Pilla, R. M., C. E. Williamson, J. Zhang, et al. 2018. "Browning-Related Decreases in Water Transparency Lead to Long-Term Increases in Surface Water Temperature and Thermal Stratification in Two Small Lakes." *Journal of Geophysical Research: Biogeosciences* 123: 1651–1665. https://doi.org/10.1029/2017JG004321.

Pitarch, J. 2020. "A Review of Secchi's Contribution to Marine Optics and the Foundation of Secchi Disk Science." *Oceanography* 33: 26–37. https://doi.org/10.5670/oceanog.2020.301.

Pitarch, J., M. Bellacicco, S. Marullo, and H. J. Van Der Woerd. 2021. "Global Maps of Forel-Ule Index, Hue Angle and Secchi Disk Depth Derived From 21 Years of Monthly ESA Ocean Colour Climate Change Initiative Data." *Earth System Science Data* 13: 481–490. https://doi.org/10.5194/essd-13-481-2021.

Pöschke, F., J. Lewandowski, C. Engelhardt, et al. 2015. "Upwelling of Deep Water During Thermal Stratification Onset—A Major Mechanism of Vertical Transport in Small Temperate Lakes in Spring?" *Water Resources Research* 51: 9612–9627. https://doi.org/10.1002/2015WR017579.

Rand, J. M., M. O. Nanko, M. B. Lykkegaard, et al. 2022. "The Human Factor: Weather Bias in Manual Lake Water Quality Monitoring." *Limnology and Oceanography: Methods* 20: 288–303. https://doi.org/10.1002/lom3.10488.

Read, J. S., K. C. Rose, L. A. Winslow, and E. K. Read. 2015. "A Method for Estimating the Diffuse Attenuation Coefficient (KdPAR) From Paired Temperature Sensors." *Limnology and*

Oceanography: Methods 13: 53–61. https://doi.org/10.1002/lom3.10006.

Rinke, K., P. Yeates, and K. O. Rothhaupt. 2010. "A Simulation Study of the Feedback of Phytoplankton on Thermal Structure Via Light Extinction." *Freshwater Biology* 55: 1674–1693. https://doi.org/10.1111/j.1365-2427.2010.02401.x.

Rodero, C., R. Bardaji, E. Olmedo, and J. Piera. 2022. "Operational Monitoring of Water Quality With a Do-It-Yourself Modular Instrument." *Frontiers in Marine Science* 9: 1004159. https://doi.org/10.3389/fmars.2022.1004159.

Rose, K. C., L. A. Winslow, J. S. Read, and G. J. A. Hansen. 2016. "Climate-Induced Warming of Lakes Can Be either Amplified or Suppressed by Trends in Water Clarity." *Limnology and Oceanography Letters* 1: 44–53. https://doi.org/10.5066/F7028PN4.

Scordo, F., C. Seitz, E. K. Suenaga, et al. 2024. "An Inexpensive Method for the Measurement of Photosynthetically Active Radiation Profiles in Waterbodies." *Aquatic Sciences* 86, no. 3: 68. https://doi.org/10.1007/s00027-024-01082-x.

Secchi, P. A. 1864. "Relazione Delle Esperienze Fatte a Bordo Della Pontificia Pirocorvetta l'immacolata Concezione Per Determinare La Trasparenza Del Mare; Memoria Del p. A. Secchi." *Il Nuovo Cimento* 20: 205–238. https://doi.org/10.1007/BF02726911.

Smith, D. G. 2001. "A Protocol for Standardizing Secchi Disk Measurements, Including Use of a Viewer Box." *Lake and Reservoir Management* 17: 90–96. https://doi.org/10.1080/07438140109353977.

Subin, Z. M., W. J. Riley, and D. Mironov. 2012. "An Improved Lake Model for Climate Simulations: Model Structure, Evaluation, and Sensitivity Analyses in CESM1." *Journal of Advances in Modeling Earth Systems* 4, no. 1: 2011MS000072. https://doi.org/10.1029/2011MS000072.

Turner, J. S., K. A. Fall, and C. T. Friedrichs. 2023. "Clarifying Water Clarity: A Call to Use Metrics Best Suited to Corresponding Research and Management Goals in Aquatic Ecosystems." *Limnology and Oceanography Letters* 8: 388–397. https://doi.org/10.1002/lol2.10301.

Tyler, J. E. 1968. "The Secchi Disc." *Limnology and Oceanography* 13, no. 1: 1–6. https://doi.org/10.4319/lo.1968.13.1.0001.

Weiskerger, C. J., M. D. Rowe, C. A. Stow, D. Stuart, and T. Johengen. 2018. "Application of the Beer–Lambert Model to Attenuation of Photosynthetically Active Radiation in a Shallow, Eutrophic Lake." *Water Resources Research* 54: 8952–8962. https://doi.org/10.1029/2018WR023024.

Wernand, M. R. 2010. "On the History of the Secchi Disc." *Journal of the European Optical Society-Rapid Publications* 5: 10013s. https://doi.org/10.2971/jeos.2010.10013s.

Yang, X., C. M. O'Reilly, J. R. Gardner, et al. 2022. "The Color of Earth's Lakes." *Geophysical Research Letters* 49, no. 18: e2022GL098925. https://doi.org/10.1029/2022GL098925.

Submitted 02 August 2024
Revised 11 February 2025
Accepted 05 March 2025